Effective temperature vs line-depth ratio for ELODIE spectra. Gravity and rotational velocity effects ⋆

K. Biazzo[1,2,⋆⋆], **A. Frasca**[1], **S. Catalano**[1], and **E. Marilli**[1]

[1] INAF - Catania Astrophysical Observatory, via S. Sofia 78, I-95123 Catania, Italy
[2] Department of Physics and Astronomy, University of Catania, via S. Sofia 78, I-95123 Catania, Italy

The dates of receipt and acceptance should be inserted later

Key words stars: fundamental parameters – stars: late-type – techniques: spectroscopy

The dependence on the temperature of photospheric line-depth ratios (LDRs) in the spectral range 6190–6280 Å is investigated by using a sample of 174 ELODIE Archive stellar spectra of luminosity class from V to III. The rotational broadening effect on LDRs is also studied. We provide useful calibrations of effective temperature versus LDRs for giant and main sequence stars with $3800 \lesssim T_{\rm eff} \lesssim 6000$ K and $v \sin i$ in the range 0–30 km s^{-1}. We found that, with the exception of very few line pairs, LDRs, measured at a spectral resolution as high as 42 000, depend on $v \sin i$ and that, by neglecting the rotational broadening effect, one can mistake the $T_{\rm eff}$ determination of ∼100 K in the worst cases.

1 Introduction

The stellar effective temperature is one of the most important astrophysical parameters. It is not easy to measure it with high accuracy and this situation worsens for stars that have already left the main sequence and that are expanding their envelopes and redistributing their angular momentum. In addition, surface inhomogeneities, such as spots and faculae can significantly affect the average temperature of active stars.

Several diagnostics, based on color indices and spectral-type classification, are available for temperature measurements, but errors greater than 100 Kelvin degrees are often encountered. On the other hand, the analysis of line profiles and their dependence upon the stellar effective temperature is a very powerful tool for the study of the photospheric temperature, as well as for the investigation of stellar surface structures.

As a matter of fact, it has been demonstrated that the ratio of the depths of two lines having different sensitivity to temperature is an excellent diagnostics for measuring small temperature differences between stars or small temperature variations of a given star. Although the effective temperature scale can be set to within a few tens of degrees, temperature differences can be measured with a precision down to a few Kelvin degrees in the most favorable cases (e.g., Gray & Johanson 1991, Strassmeier & Schordan 2000, Gray & Brown 2001, Catalano et al. 2002a, 2002b). This allows putting a star sample in a "relative" temperature scale or to detect tiny temperature variations in individual stars. Starspot temperatures from line-depth ratios (LDRs) variations, indeed, have been determined in the slowly rotating dwarf star σ Draconis (Gray et al. 1992), in the very young and rapidly rotating star LQ Hydrae (Strassmeier et al. 1993), in some young solar-type stars (Biazzo et al. 2007), and in three single-lined RS CVn binaries (Frasca et al. 2005). However, all these works do not explicitly take into account the effects of stellar rotation on spectral line depths and consequently on LDRs.

In the present work, we primarily explore the influence of the rotational velocity on LDRs and provide calibration relations between individual LDRs and effective temperature at different rotation velocities for high-resolution spectra ($R = 42\,000$) taken from the ELODIE Archive (Moultaka et al. 2004), taking also into account the effect of gravity.

The effect of slightly different metallicity for the stars in our sample is also examined. Its influence on LDRs is found to be negligible for stars around solar metallicity (within ± 0.3).

2 The star sample

2.1 Sample selection

We selected 174 stellar spectra of giant and main sequence stars (MS) from the on-line ELODIE Archive (Moultaka et al. 2004). Their spectral types range from F5 to M0 (Hoffleit & Warren 1991). The criteria for the choice of the stellar sample are the following:

– low rotation rate, $v \sin i \lesssim 5$ km s^{-1} (values mainly taken from Bernacca & Perinotto 1970, de Medeiros & Mayor 1999, Glebocki et al. 2000);

⋆ Based on spectral data retrieved from the ELODIE Archive at Observatoire de Haute-Provence (OHP).

⋆⋆ Corresponding author: e-mail: katia.biazzo@oact.inaf.it.

– good Hipparcos parallaxes (π) with errors less than 15% (ESA 1997);
– accurate $B-V$ color indices (Mermilliod & Mermilliod 1998) ranging from 0.49 to 1.37 for the 102 MS stars and from 0.64 to 1.54 for the 72 giant stars;
– nearly solar metallicity, [Fe/H]=0.0 ± 0.3 (Soubiran et al. 1998).

2.2 Effective temperature and luminosity

In order to determine the $T_{\rm eff}$ and luminosity of the stars in our sample and to put them onto the HR diagram, it is necessary to evaluate the interstellar extinction (A_V) and reddening (E_{B-V}). We have evaluated A_V from the star distance, assuming a mean extinction of 1.7 mag/kpc for stars on the galactic plane ($|b| < 5°$) and of 0.7 mag/kpc for stars out of the plane ($|b| > 5°$). The reddening was estimated according to the standard law $A_V = 3.1\,E_{B-V}$ (Savage & Mathis 1979), with E_{B-V} color excess. However, the color excess of these nearby stars is always less than $0\overset{\rm m}{.}03$ for MS stars and less than $0\overset{\rm m}{.}09$ for giant stars. The only two exceptions are HD 176737 and HD 54489 where $E_{B-V} \sim 0.20$ since they have $|b| < 5°$ and $\pi < 3$ mas. Fig. 1 shows the distributions of the de-reddened color $(B-V)_0$ for the MS and giant stars. The de-reddened V magnitude was converted into absolute magnitude M_V through the parallax and subsequently into bolometric magnitude by means of the bolometric corrections tabulated by Flower (1996) as a function of the effective temperature. A solar bolometric magnitude of $M_{\rm bol} = 4.64$ (Cox 2000) was used to express the stellar luminosity in solar units. From $(B-V)_0$ values we have deduced the effective temperature by means of the following empirical relation given by Gray (2005) and valid for $0.00 \leq (B-V)_0 \lesssim 1.5$:

$$\log T_{\rm eff} = 3.981 - 0.4728(B-V)_0 + 0.2434(B-V)_0^2 - 0.062(B-V)_0^3 \quad (1)$$

We have verified the consistency of $T_{\rm eff}$ values derived in this way with those listed by Prugniel & Soubiran (2001) and compiled from the literature (Fig. 2). The latter temperatures appear to be systematically lower than Gray's temperatures by about 120 K, on average. The root mean square (rms) of data compared to the linear fits is around 130 K both for giant and MS stars. This comparison allows us to estimate an average temperature uncertainty of about 100–150 K for the FGK stars of our sample, as already found in previous studies (see, e.g., Gray 2005, and references therein). We find analogous results by plotting the $T_{\rm eff}$ derived from Gray's relation with those obtained by means of the $T_{\rm eff}$–$(V-I)$ calibration by Alonso et al. (1996, 1999). After several tests made on the LDR–$T_{\rm eff}$ calibrations, we have chosen to use Gray's effective temperatures for the following analysis, because they give the smallest scatter in the calibrations (rms$\simeq$0.13, 0.14, and 0.06 for Prugniel & Soubiran, Alonso et al., and Gray temperature sets, respectively). Anyway, the use of Alonso et al.'s temperature scale, instead of Gray's scale, does not affect significantly the LDR–$T_{\rm eff}$ calibrations.

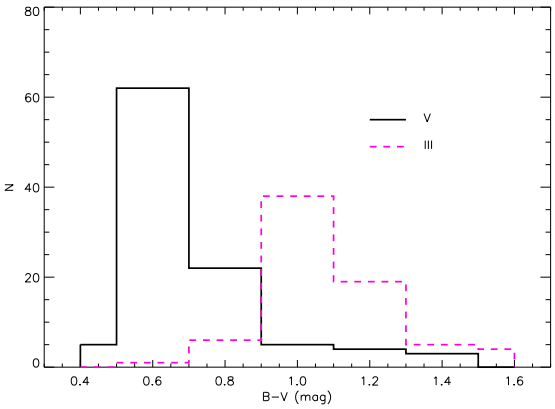

Fig. 1 $B-V$ distribution of the giant (III) and MS (V) calibration stars.

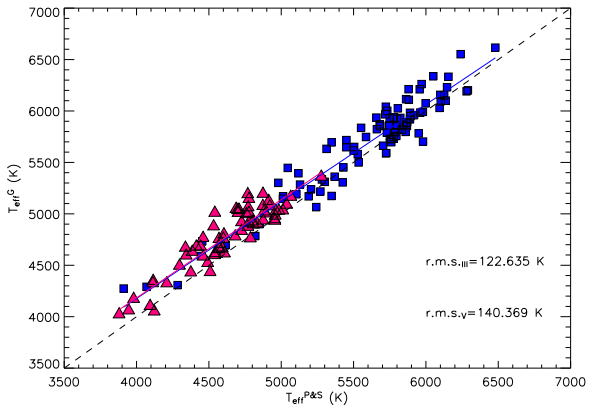

Fig. 2 Comparison between the effective temperatures of the giant (triangles) and MS (squares) stars obtained using the Gray's calibration (Gray 2005) and those listed by Prugniel & Soubiran (2001). The two continuous lines represent the linear fits to the two star groups, while the dashed line is the bisector.

The position onto the Hertzsprung-Russel (HR) diagram of the ELODIE stars used in this work is shown in Fig. 3 together with the evolutionary tracks and isochrones calculated by Girardi et al. (2000).

3 LDR analysis and results

3.1 Line identification

Within the visible region of cool star spectra, there are several pairs of lines suitable for temperature determination. Most works are based on line pairs in the spectral domain around 6200 Å (Gray & Johanson 1991, Gray & Brown 2001, Catalano et al. 2002a, 2002b, Biazzo 2006) and 6400 Å (Strassmeier & Fekel 1990, Strassmeier & Schordan 2000).

For this work, several spectral lines have been chosen in the 6190–6280 Å range. A sample of ELODIE spectra

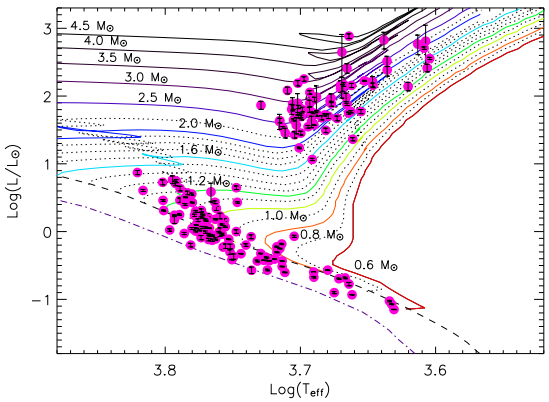

Fig. 3 HR diagram of the stars in our sample. The evolutionary tracks for different masses are taken from Girardi et al. (2000) and are shown by continuous and dotted lines. The isochrones at an age of 6.31×10^7 yrs (ZAMS) with $Z = 0.019$ ([Fe/H]=0) and $Z = 0.01$ ([Fe/H]~ -0.3) are also displayed with dashed and dash-dotted lines, respectively.

of different spectral types is shown in Fig. 4. The lines were identified through the solar (Moore et al. 1966) and Arcturus (Griffin 1968) atlases, choosing those appearing unblended at the very high resolution of the aforementioned atlases. The chosen lines, their excitation potential χ (Moore et al. 1966) and ionization energy I (Allen 1973) in electron volts are listed in Table 1 together with a code number in the fifth column. The lines for each ratio are chosen to be close together in order to minimize the errors in the continuum setting. Fifteen line ratios are used altogether in this work. Each spectral line has an intensity depending specifically on temperature and gravity (or electronic pressure) through the line and continuum absorption coefficients (l_ν and κ_ν). These parameters are related to the excitation and ionization potentials, χ and I, by means of Boltzmann and Saha equations. For these reasons, for example, the lines λ6243.11 V I and λ6247.56 Fe II change in opposite directions with temperature, as displayed in Fig. 4, where the effect of temperature and gravity on line intensities is apparent.

The measure of line depths (d), LDRs (r), and the evaluation of errors has been carried out according to the guidelines of Catalano et al. (2002a).

3.2 Metallicity effect

Before proceeding with the calibration, it is important to evaluate the dependence of line-depth ratios on metallicity. Gray (1994) has investigated the influence of metallicity on color indices, finding an empirical relation between $B-V$ and the logarithm of the iron abundance normalized to the Sun ([Fe/H]). A calibration relation between $B-V$ and $T_{\rm eff}$ depending on [Fe/H] has been also proposed by Alonso et al. (1999). However, the $B-V$ color index is only very slightly dependent on [Fe/H] for stars of nearly solar metallicity. Furthermore, Gray (1994) did not find any dependence on [Fe/H] for LDRs of weak lines and only a very

Table 1 Spectral lines. Each line printed in italics is fully blended with the preceding one.

λ (Å)	Element	χ (eV)	I (eV)	Code
6199.19	V I	0.29	6.74	1
6200.32	Fe I	2.61	7.87	2
6210.67	Sc I	0.00	6.54	3
6213.44	Fe I	2.22	7.87	4
6213.83	V I	0.30	6.74	5
6215.15	Fe I	4.19	7.87	6
6215.22	*Ti I*	*2.69*	*6.82*	
6216.36	V I	0.28	6.74	7
6223.99	Ni I	4.10	7.63	8
6224.51	V I	0.29	6.74	9
6232.65	Fe I	3.65	7.87	10
6233.20	V I	0.28	6.74	11
6242.84	V I	0.26	6.74	12
6243.11	V I	0.30	6.74	13
6243.82	Si I	5.61	8.15	14
6246.33	Fe I	3.60	7.87	15
6247.56	Fe II	3.89	16.18	16
6251.83	V I	0.29	6.74	17
6252.57	Fe I	2.40	7.87	18
6255.95	Fe I	?	7.87	19
6256.35	Ni I	1.68	7.63	20
6256.36	*Fe I*	*2.45*	*7.87*	
6256.89	V I	0.28	6.74	21
6265.14	Fe I	2.18	7.87	22
6266.33	V I	0.28	6.74	23
6268.87	V I	0.30	6.74	24
6270.23	Fe I	2.86	7.87	25
6274.66	V I	0.27	6.74	26

weak dependence for the line pair λ6251.83 V I–λ6252.57 Fe I, amounting to about ±20 K for [Fe/H] in the range ±0.3. Since all the stars analysed in this work have metallicities close to the solar value (within ±0.3) and taking also into account the large uncertainty on many [Fe/H] literature data, no correction for this parameter has been applied. Anyway, given the high number of stars in our sample, possible residual effects due to small metallicity differences not properly accounted for are not expected to significantly affect our calibration.

3.3 Gravity effect

Line depth ratios are sensitive to gravity due to the dependence on the electron pressure of the H^- bound-free continuum absorption coefficient. As a consequence, to determine the temperature of stars with different gravity, such as giants and MS, it is necessary to evaluate this dependence and/or to set appropriate temperature scales (Biazzo 2001).

For this reason, in the present work different $r-T_{\rm eff}$ calibrations have been performed for MS and giant stars. We have taken into account the gravity spread in each sample in the following way:

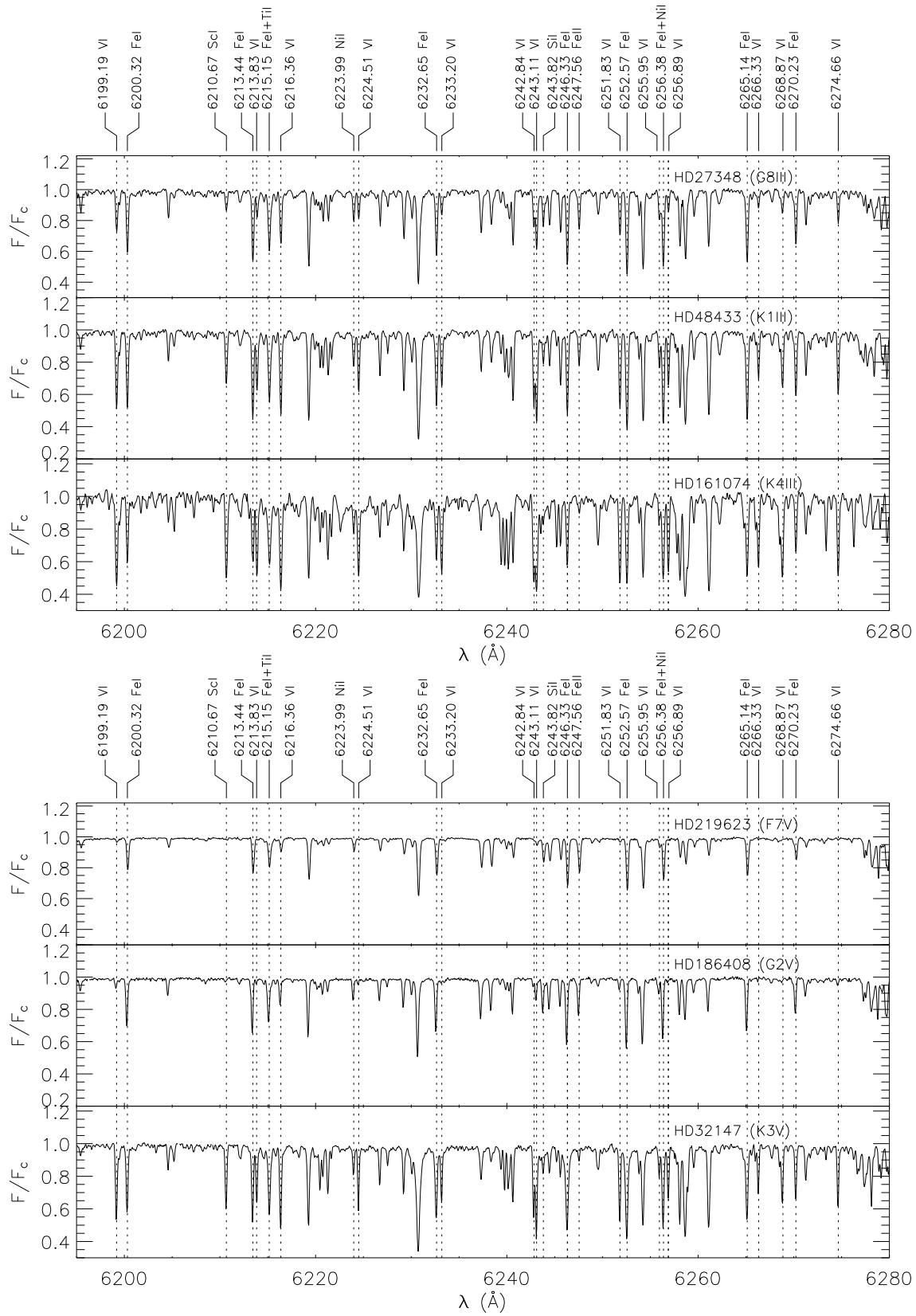

Fig. 4 Three representative normalized spectra for giant (upper panel) and MS (bottom panel) stars. Temperature decreases from top to bottom. The spectral lines used for the LDR computation are labeled with their wavelength (in Å), chemical element and ionization level. The lines, with low excitation potential, such as λ6210.67 Sc I or λ6266.33 V I, increase their depth with decreasing temperature, while the λ6247.56 Fe II line, with high excitation potential, shows an opposite behaviour. The lines with intermediate χ, such as λ6256.35 Ni I, don't display any relevant variation in this temperature range.

i. for MS stars we have considered the difference ΔL between their luminosity and that of ZAMS stars of the same color (Fig. 3) as a gravity index;
ii. for giant stars we have computed their gravity, $\log g$, according to the evolutionary tracks of Girardi et al. (2000).

Then, the residuals $\Delta r_{\rm MS,GIA}$ of LDRs compared to the fits in the $(B-V)_0 - r$ plane have been plotted against ΔL and $\log g$ for MS and giant stars, respectively. A linear fit to the data provides very small positive slopes, indicating slightly increasing LDRs with gravity (Fig. 5). The linear fit was obtained by means of POLY_FIT, an IDL routine using matrix inversion, which performs a weighted least-square polynomial fit with error estimates. If a and b are the intercept and the slope of these linear fits, respectively, the gravity-corrected line-depth ratio, $r_{\rm c}$, is

$$r_{\rm c} = r - (a + b\Delta L), \quad (2)$$

for MS stars and

$$r_{\rm c} = r - (a + b\log g), \quad (3)$$

for giant stars. In Eq. 2 and 3, r is the observed LDR. The final polynomial fits to the corrected LDRs are of the type

$$T_{\rm eff} = c_0 + c_1 r_{\rm c} + ... + c_n r_{\rm c}^n,$$

both for MS and giant stars, with c_0, ..., c_n coefficients of the polynomial fits. An example of calibration is illustrated in Fig. 6 and the polynomial fit coefficients are listed in Table 2 for the 15 different line pairs.

With the aim of verifying the internal consistency of our method, we have computed the effective temperature of each star coming from each $r_{\rm c} - T_{\rm eff}$ calibration and we have carried out the weighted average on all the 15 LDR. The resulting $< T_{\rm eff} >$ are plotted as a function of $(B-V)_0$ in Fig. 7, together with the following polynomial fit on the points (continuous line):

$$\begin{aligned}\log < T_{\rm eff} > \; &= \; 3.85478 - 0.0582469(B-V)_0 \\ &- \; 0.1883(B-V)_0^2 + 0.0823(B-V)_0^3\end{aligned}$$

In the range $0.5 \lesssim (B-V)_0 \lesssim 1.5$, our $< T_{\rm eff} > -(B-V)_0$ calibration is perfectly consistent with the one expressed in Eq. 1 and obtained by Gray (2005). The data scatter is obviously larger than the individual errors in $< T_{\rm eff} >$ (originating from the LDR errors), due to the errors in the $B-V$ measurements and to the residual dependence of $B-V$ on the stellar parameters other than the effective temperature, like metallicity and microturbulence.

The values of $< T_{\rm eff} >$, L and $r_{\rm c}$ for all the standard stars are listed in Table 5[1].

[1] Table 5 is only available in electronic form at the Web site http://cdsads.u-strasbg.fr/.

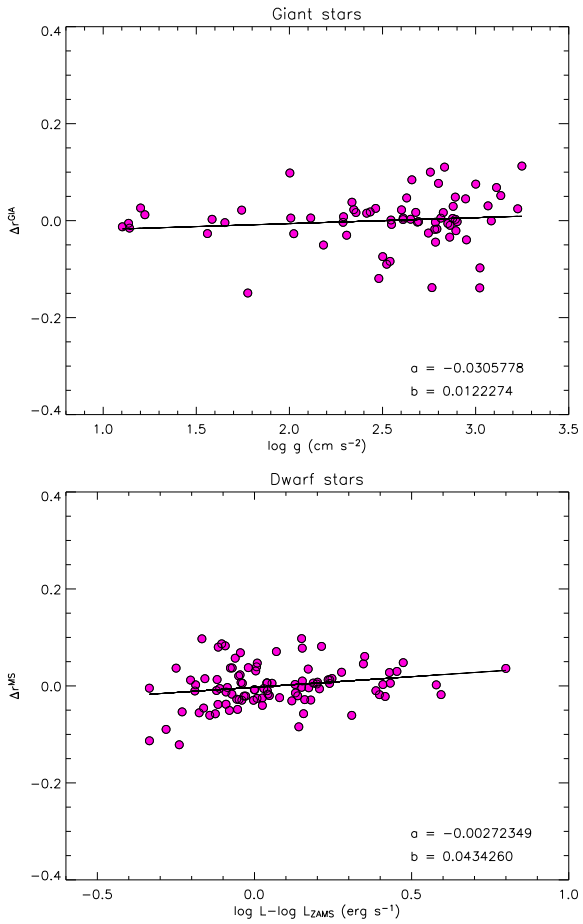

Fig. 5 Examples of the residuals of the LDR λ6252 V I-λ6253 Fe I compared to the polynomial fit as a function of the gravity index (dots). The continuous lines represent linear fits to the data of giants and MS stars, respectively.

3.4 Rotational broadening effect

In a moderately rotating star, the depth at the line center decreases with increasing $v \sin i$ at a rate depending on the line characteristics. Following Stift & Strassmeier (1995), in a weak line for which the saturation effects are very small, the residual intensity directly reflects the run of the opacity profile with frequency. A strong line, in contrast, behaves differently, because saturation leads to a contribution to the intensity at the line center that remains fairly high over a considerable part of the stellar disk, resulting in a slow decrease in the central line intensity with $v \sin i$. This implies that if two lines are of comparable strength and do not differ radically in the broadening parameters, the LDR will not depend on rotation. Stift & Strassmeier (1995) investigated the dependence of the LDR on rotation by synthesizing the spectral region containing the λ6252 V I and λ6253 Fe I lines in a grid of atmospheric models (Kurucz 1993) for main-sequence stars with $v \sin i$ values ranging from 0.0 to 6.0 km s^{-1}. They estimated that, for a fixed microturbulence, the rotation dependence is always present at all tem-

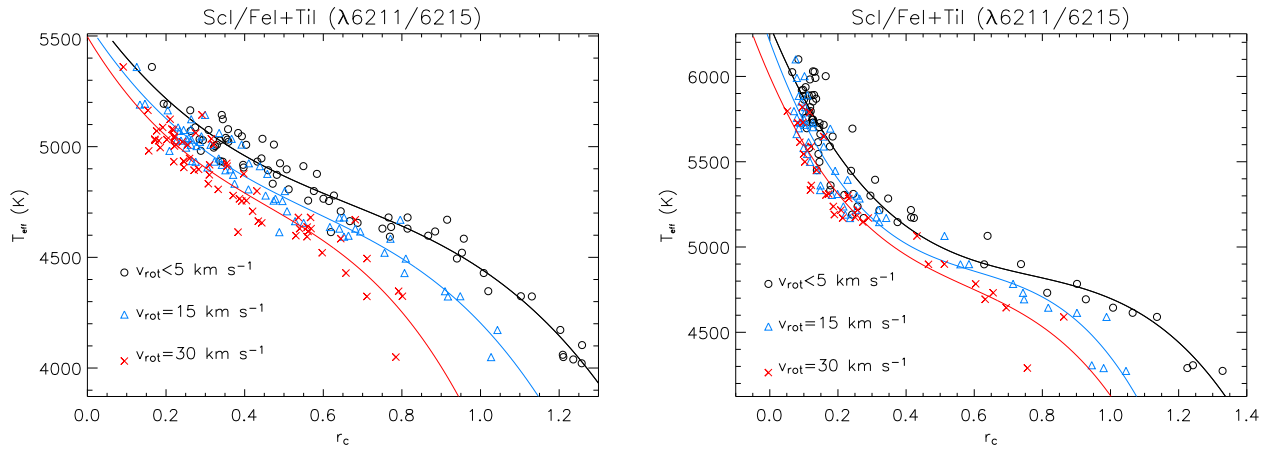

Fig. 6 $r_c - T_{\rm eff}$ calibration for the line pair λ6211 Sc I-λ6215 Fe I+Ti I at different $v \sin i$'s (open circles: $v \sin i$=0 km s^{-1}; triangles: $v \sin i$=15 km s^{-1}; crosses: $v \sin i$=30 km s^{-1}) for giant stars (*left panel*) and MS stars (*right panel*).

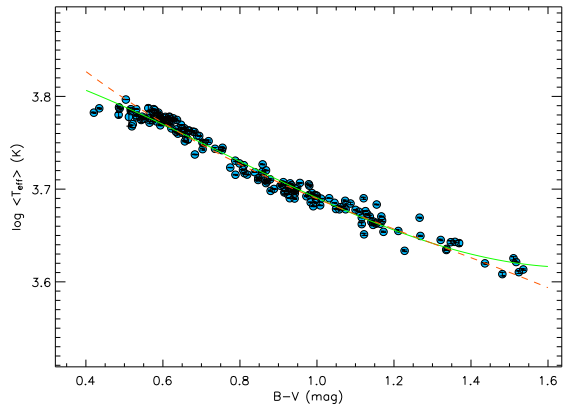

Fig. 7 $< T_{\rm eff} >$ of the standards as a function of the de-reddened $B - V$. The continuous and dashed lines are referred to our and Gray's calibrations, respectively.

peratures (from 3500 to 6000 K) for a $v \sin i \geq 4 - 5$ km s^{-1}.

We find similar results computing the LDRs obtained from high-resolution synthetic spectra. In particular, we have considered the Synthetic Stellar Library described and made available by Coelho et al. (2005), which contains spectra synthesized by adopting the model atmospheres of Castelli & Kurucz (2003). These spectra are sampled at 0.02 Å, range from the near-ultraviolet (300 nm) to the near-infrared (1.8 μm), and cover the following grid of parameters: 3500 $\leq T_{\rm eff} \leq$7000 K, 0.0 $\leq \log g \leq$ 5.0, $-2.5 \leq$[Fe/H]$\leq$+0.5, α-enhanced [α/Fe]=0.0, 0.4 and microturbulent velocity v_t=1.0, 1.8, 2.5 km s^{-1}. In Fig. 8 we show, as an example, the behaviour of synthetic LDRs with $v \sin i$ at three different $T_{\rm eff}$ for the line pair λ6211 Sc I-λ6215 Fe I+Ti I. The synthetic-LDR for this couple decreases with the increase in $v \sin i$ from 0 to about 20 km s^{-1} and then remains nearly constant. This behaviour is apparent in all the three temperatures displayed in Fig. 8, and is more evident in the lowest one. Neglecting this effect, a systematic error in the effective temperature can arise. For instance, if we use the $r_c - T_{\rm eff}$ calibration obtained by us at $v \sin i$=0 km s^{-1} for a giant star with $T_{\rm eff}$=4750 K and $v \sin i$= 20 km s^{-1}, we overestimate its effective temperature by about 80 K. As a consequence, this LDR appears to be quite sensitive to the rotation velocity in the range 0–20 km s^{-1}. Thus, the rotational broadening must be taken into account to perform a reliable calibration for this as well as for several other LDRs.

To study in detail the influence of rotational broadening on LDRs, we have computed the LDRs of our star sample broadening the corresponding spectra at different rotation velocities from 0 to 30 km s^{-1} in steps of 5 km s^{-1}. The LDR calculation has been carried out with a simple code written in IDL[2]. The code first convolves the spectrum with the required rotational profile and then, automatically, computes the 15 LDRs in the selected wavelength range.

An example of an $r_c - T_{\rm eff}$ calibration (λ6211 Sc I-λ6215 Fe I+Ti I) both for giant and MS stars is displayed in Fig. 6, where only the calibrations for three $v \sin i$ values (0, 15, and 30 km s^{-1}) are shown. We find that for some LDRs the effects of the broadening are already visible at 5 km s^{-1}, while some other LDRs are practically not affected by the rotational broadening. The main characteristics of these calibrations can be summarized as follows.

- Because of blending problems, for some pairs it is not possible to broaden the lines at any rotational velocity (e.g., λ6214 V I-λ6213 Fe I, λ6233 V I-λ6232 Fe I, λ6242 V I-λ6244 Si I, λ6252 V I-λ6253 Fe I, λ6257 V I-λ6255 Fe I, λ6257 V I-λ6256 Fe I+Ni I).
- Some LDRs seem not to suffer from rotational broadening effects in almost all the effective temperature ranges (for example λ6199 V I-λ6200 Fe I, λ6214 V I-λ6213 Fe I, λ6275 V I-λ6270 Fe I), as expected for weak lines.

[2] IDL (Interactive Data Language) is a trademark of Research Systems Incorporated (RSI).

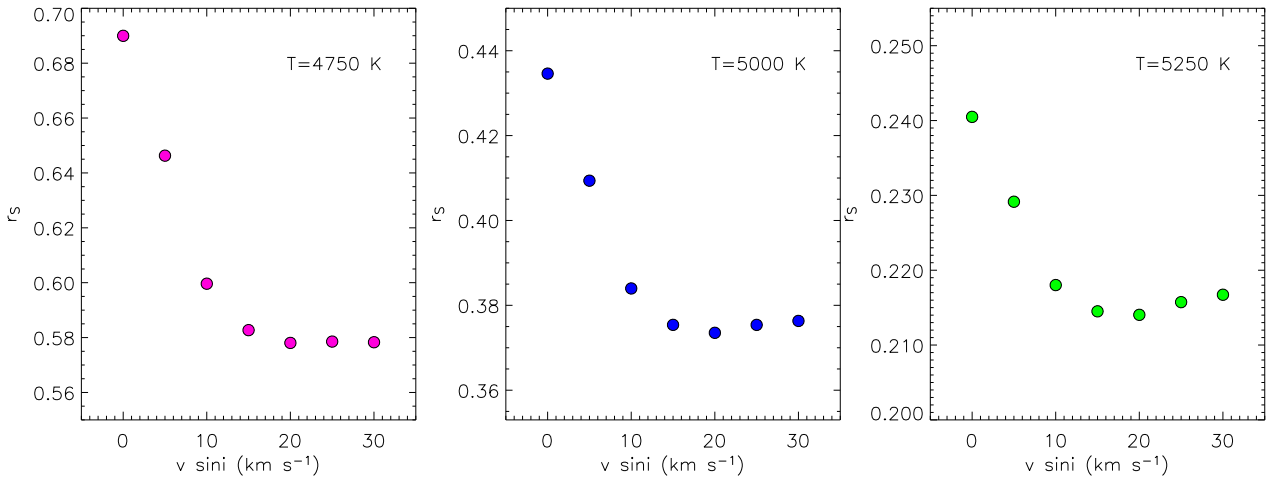

Fig. 8 Synthetic LDRs at 3 different $T_{\rm eff}$ as a function of $v \sin i$ for the line pair λ6211 Sc I-λ6215 Fe I+Ti I. The synthetic spectra are referred to a star with $\log g$=2.5, [Fe/H]=0.0, [α/Fe]=0.0, v_t=1.8, and have been degraded to the same resolution of ELODIE.

– Some line pairs show variation due to rotational broadening for a temperature lower than about 4500 K and 5000 K for giant and MS stars, respectively (e.g., λ6243 V I-λ6247 Fe II, λ6269 V I-λ6270 Fe I).
– Other couples display changes at any temperature (e.g., λ6211 Sc I-λ6215 Fe I+Ti I, λ6216 V I-λ6215 Fe I+Ti I, λ6252 V I-λ6253 Fe I, λ6266 V I-λ6265 Fe I).
– The slope of $r_{\rm c} - T_{\rm eff}$ calibration in some ratios decreases with the increase in the rotation (e.g., λ6243 V I-λ6246 Fe I), while in some other ratios increases with the rotation (e.g., λ6216 V I-λ6215 Fe I+Ti I).
– In any case, the variation of the slope with $v \sin i$ seems to be more evident for giant stars compared to MS stars (e.g., λ6243 V I-λ6246 Fe I and λ6269 V I-λ6270 Fe I). This behaviour can be due to the fact that the giants have narrower lines compared to MS stars, due to their lower atmospheric density. As a consequence, they appear to be sensitive to the rotational broadening, while the gravity broadening in MS stars is comparable to the rotational broadening at low rotational velocity and the effect on LDR comes out to be less prominent.

3.4.1 Temperature sensitivity on LDR

In order to measure the temperature sensitivity of each LDR, the slopes $\frac{{\rm d}T}{{\rm d}r_{\rm c}}$ of the polynomial fits have been calculated. The $\frac{{\rm d}T}{{\rm d}r_{\rm c}}$ absolute values at a temperature of 5000 K are listed in Table 2 for the calibrations of the giant and MS stars not rotationally broadened. Values of about 10–30 K and, in some case, even smaller, have been found for a 0.01 variation of $r_{\rm c}$, which represents the typical uncertainty for the LDR determination in well-exposed spectra. Stars below 4000 K and above 6200 K have the most uncertain temperatures because of the influence of molecular bands in the coolest stars and the very small depths of the low-excitation lines in the hottest stars of our sample, respectively.

Thus, the temperature sensitivity changes from an LDR to another one, but it is also a function of the rotational velocity. Fig. 9 displays an example of the variation of the temperature sensitivity with the rotational velocity of the couple λ6211 Sc I-λ6215 Fe I+Ti I obtained for the giant calibration. For this ratio, the temperature sensitivity decreases with the increasing rotational broadening. As we mentioned before, other LDRs display different behaviours of the temperature sensitivity as a function of $v \sin i$.

The coefficients ($c_0, ..., c_n$) of the fits and the values of $\frac{{\rm d}T}{{\rm d}r_{\rm c}}$ and rms obtained at $v \sin i$=0, 15, and 30 km s^{-1} are listed in Tables 2, 3 4, respectively.

4 Conclusion

In this work we have performed LDR–$T_{\rm eff}$ calibrations from high-resolution spectra taking into account the corrections for the gravity effect and the rotational broadening. To our knowledge, this is the first work in which the dependence of LDRs on rotational velocity has been considered on real spectra. In previous studies, this dependence had not been taken into account, also following Gray & Johanson's (1991) early suggestions that considered the effect of $v \sin i$ to be negligible. Here we demonstrate that the rotational broadening effect is already evident at 5 km s^{-1} both in synthetic and real spectra of cool stars. Its effect can be neglected only in particular temperature domains and for a few line pairs. In other situations, the dependency of LDRs on $v \sin i$ must be properly taken into account, at least at a spectral resolution as high as 42 000. We show that neglecting this effect can lead to temperature overestimates as high as $\approx$100 K.

This paper provides calibrations that can be used for temperature determinations of stars with $0 \leq v \sin i \lesssim 30$ km s^{-1} and observed with ELODIE as well as with other

Table 2 Coefficients of the fits $T_{\rm eff} = c_0 + c_1 r_{\rm c} + ... + c_n r_{\rm c}^n$ for the ELODIE spectra not rotationally broadened.

GIANT STARS								
LDR	1/2	3/6	5/4	7/6	9/8	11/10	12/14	13/15
c_0	5658.52	5630.37	5357.34	8808.49	4976.68	5328.31	5375.97	5435.02
c_1	−1565.89	−2563.00	−846.737	−10484.1	697.119	−749.330	−292.110	−8.57992
c_2	1384.63	2766.46	−176.810	10403.9	−849.779	−150.672	−25.7998	−654.941
c_3	−807.719	−1384.76	−80.6700	−3804.58	184.978	−3.71716	0.715242	
$0.01\,\lvert\frac{\mathrm{d}T}{\mathrm{d}r_{\rm c}}\rvert_{5000\,\rm K}$	10.4	11.0	12.4	14.9	5.2	10.9	4.0	12.8
rms	0.080	0.060	0.070	0.071	0.081	0.078	0.085	0.068
LDR	13/16	17/18	21/19	21/20	23/22	24/25	26/25	
c_0	5479.94	5630.09	5204.23	5407.48	5324.25	5346.80	5335.75	
c_1	−325.954	−1935.08	−53.5851	−2091.73	−1625.05	−1054.34	−327.402	
c_2	4.71410	2496.75	−325.674	2640.38	1431.70	619.856	−313.672	
c_3	1.43373	−1976.03	74.5653	−1956.14	−1193.13	−343.396	−42.0121	
$0.01\,\lvert\frac{\mathrm{d}T}{\mathrm{d}r_{\rm c}}\rvert_{5000\,\rm K}$	4.1	13.2	6.3	12.9	13.9	9.2	10.1	
rms	0.070	0.054	0.068	0.062	0.063	0.081	0.081	
DWARF STARS								
LDR	1/2	3/6	5/4	7/6	9/8	11/10	12/14	13/15
c_0	6592.19	6298.64	6303.41	8075.38	6181.66	6204.32	6122.76	6583.91
c_1	−4053.01	−4813.87	−5018.31	−6053.31	−1077.50	−3855.13	−895.008	−3240.32
c_2	4020.50	5670.56	6604.68	4843.37	197.649	3379.47	158.882	2763.93
c_3	−1663.63	−2457.28	−3562.99	−1688.39	−7.73603	−1175.00	−8.65057	−1211.49
$0.01\,\lvert\frac{\mathrm{d}T}{\mathrm{d}r_{\rm c}}\rvert_{5000\,\rm K}$	11.0	10.1	13.4	15.7	4.5	12.4	2.8	13.2
rms	0.065	0.060	0.040	0.057	0.085	0.047	0.087	0.049
LDR	13/16	17/18	21/19	21/20	23/22	24/25	26/25	
c_0	6250.15	6486.68	6178.37	6210.10	6228.96	6120.07	6271.19	
c_1	−732.154	−5065.09	−1203.98	−5244.93	−6031.24	−2734.59	−1994.09	
c_2	143.714	7059.62	261.964	6959.06	9450.38	1909.74	716.031	
c_3	−9.97940	−4105.26	−19.2823	−3796.17	−5981.44	−559.915	−138.664	
$0.01\,\lvert\frac{\mathrm{d}T}{\mathrm{d}r_{\rm c}}\rvert_{5000\,\rm K}$	1.4	15.2	5.0	16.5	18.0	8.5	9.8	
rms	0.074	0.043	0.067	0.047	0.053	0.067	0.076	

spectrographs at a similar resolution. We have shown that all the LDRs examined in the present paper display a good sensitivity to the effective temperature which allows us to reach an uncertainty lower than 10–15 K at $R = 42\,000$ for stars rotating up to $v \sin i$=30 km s^{-1}. The simultaneous use of several LDRs allows us to improve the temperature sensitivity and to fully detect and analyse effective temperature modulations produced by cool starspots in active stars, as we have already shown in previous works (Frasca et al. 2005, Biazzo et al. 2007).

Acknowledgements. This work has been supported by the Italian National Institute for Astrophysics (INAF), by the Italian *Ministero dell'Istruzione, Università e Ricerca* (MIUR) and by the *Regione Sicilia* which are gratefully acknowledged. We thank the referee for useful suggestions. We are also grateful to Mrs. Luigia Santagati for the English revision of the text. This research has made use of SIMBAD and VIZIER databases, operated at CDS, Strasbourg, France.

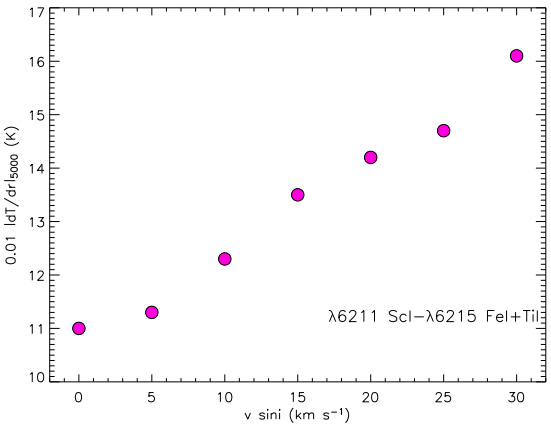

Fig. 9 Example of variation of the temperature sensitivity with the rotational velocity obtained for the giant calibration λ6211 Sc I-λ6215 Fe I+Ti I.

References

Allen, C.W.: 1973, *Astrophysical Quantities*, London: Athlone
Alonso, A., Arribas, S., Martínez-Roger, C.: 1996, A&A 313, 873
Alonso, A., Arribas, S., Martínez-Roger, C.: 1999, A&A 140, 261
Bernacca, P.L., Perinotto, M.: 1970, Contr. Oss. Astrof. Padova in Asiago, 239
Biazzo, K.: 2001, Master Thesis, Catania University
Biazzo, K.: 2006, Ph.D. Thesis, Catania University
Biazzo, K., Frasca, A., Henry, G.W. et al.: 2007, ApJ 656, 474
Castelli, F., Kurucz, R.L.: 2003, in *Modelling of Stellar Atmospheres, IAU Symp., No. 210, Poster Proc., ed. Piskunov N., Weiss W.W., Gray, D.F., A20*

Table 3 Coefficients of the fits $T_{\rm eff} = c_0 + c_1 r_{\rm c} + ... + c_n r_{\rm c}^n$ for the ELODIE spectra rotationally broadened to 15 km s^{-1}. The empty columns relate to the line pairs completely blended at this rotational velocity.

GIANT STARS								
LDR	1/2	3/6	5/4	7/6	9/8	11/10	12/14	13/15
c_0	5249.84	5559.50		8090.67	5453.71	5355.55		5662.56
c_1	245.810	−2741.36		−9105.81	−489.599	−879.618		−670.393
c_2	−1064.84	3273.61		9705.52	−34.6856	−138.541		−13.6821
c_3	306.601	−1888.48		−3948.66	33.7288	35.1345		
$0.01\,\lvert\frac{{\rm d}T}{{\rm d}r_{\rm c}}\rvert_{5000\,{\rm K}}$	9.8	13.5		15.6	5.1	12.6		8.0
rms	0.090	0.057		0.065	0.087	0.068		0.070
LDR	13/16	17/18	21/19	21/20	23/22	24/25	26/25	
c_0	5400.03	5051.44		5605.92	5297.24	5237.87	5202.02	
c_1	−231.533	−1505.89		−3632.92	−1585.45	−526.586	203.540	
c_2	13.1768	4285.89		5882.55	940.850	−111.045	−1183.49	
c_3	−0.368023	−1829.64		−4511.96	−817.658	47.8455	391.671	
$0.01\,\lvert\frac{{\rm d}T}{{\rm d}r_{\rm c}}\rvert_{5000\,{\rm K}}$	2.4	15.5		15.9	15.8	7.9	10.0	
rms	0.072	0.055		0.050	0.056	0.087	0.088	
DWARF STARS								
LDR	1/2	3/6	5/4	7/6	9/8	11/10	12/14	13/15
c_0	6537.09	6205.81		7824.72	6216.99	6451.17		6522.90
c_1	−3721.86	−5454.44		−5415.18	−1442.34	−5424.86		−2833.56
c_2	3167.41	7964.98		3678.15	532.435	5770.74		1687.54
c_3	−1119.43	−4361.33		−1198.04	−70.4289	−2439.22		−485.220
$0.01\,\lvert\frac{{\rm d}T}{{\rm d}r_{\rm c}}\rvert_{5000\,{\rm K}}$	10.7	11.8		17.9	3.2	16.0		11.0
rms	0.061	0.054		0.048	0.089	0.036		0.053
LDR	13/16	17/18	21/19	21/20	23/22	24/25	26/25	
c_0	6194.16	6312.44		6347.22	5964.93	5988.72	6264.03	
c_1	−549.734	−4404.66		−7231.99	−4180.21	−2177.96	−2135.85	
c_2	83.9286	5255.34		12331.5	4047.15	1527.77	1057.32	
c_3	−4.27056	−3379.88		−8240.08	−1716.93	−483.352	−322.180	
$0.01\,\lvert\frac{{\rm d}T}{{\rm d}r_{\rm c}}\rvert_{5000\,{\rm K}}$	1.0	18.6		16.4	18.7	6.9	10.1	
rms	0.075	0.033		0.053	0.049	0.082	0.087	

Catalano, S., Biazzo, K., Frasca, A., Marilli, E.: 2002a, A&A 394, 1009

Catalano, S., Biazzo, K., Frasca, A. et al.: 2002b, AN 323, 260

Coelho, P., Barcuy, B., Meléndez, J. et al.: 2005, A&A 443, 735

Cox, A.N.: 2000, *Allen's Astrophysical Quantities*, 4$^{\rm th}$ ed., New York: AIP Press and Springer-Verlag

de Medeiros, J.R., Mayor, M.: 1999, A&AS 139, 433

ESA: 1997, *The Hipparcos and Tycho Catalog*, ESA SP-1200

Flower, P.J.: 1996, ApJ 469, 355

Frasca, A., Biazzo, K., Catalano, S. et al.: 2005, A&A 432, 647

Girardi, L., Bressan, A., Bertelli, G., Chiosi, C.: 2000, A&AS 141, 371

Glebocki, R., Gnacinski, P., Stawikowski, A.: 2000, Acta Astron. 50, 509

Gray, D.F.: 1994, PASP 106, 1248

Gray, D.F.: 2005, *The Observation and Analysis of Stellar Photospheres*, 3$^{\rm rd}$ ed., Cambridge University Press

Gray, D.F., Johanson, H.L.: 1991, ApJ 103, 439

Gray, D.F., Baliunas, S.L., Lockwood, G.W. et al.: 1992, ApJ 400, 681

Gray, D.F., Brown, K.: 2001, PASP 113, 723

Griffin, R.F.: 1968, *A Photometric Atlas of the Spectrum of Arcturus: λ 3600–8825 Å*, Cambridge Philosophsical Society

Hoffleit, D., Warren, W.H.Jr.: 1991, *The Bright Star Catalogue*, 5$^{\rm th}$ ed. riv., http://cdsweb.u-strasbg.fr/cats/Cats.htx

Kurucz, R.L.: 1993, *ATLAS9 Stellar Atmosphere Programs and 2 km s^{-1} grid*, Kurucz CD-ROM No. 13

Mermilliod, J.-C., Mermilliod, M.: 1998, http://obswww.unige.ch/gcpd/cgi-bin/photoSys.cgi

Moore, C.E., Minnaert, M.G.J., Houtgast, J.: 1966, *The Solar Spectrum 2935 Å to 8770 Å*, National Bureau of Standards: Washington, Monograph 61

Moultaka, J., Ilovaisky, S.A., Prugniel, P., Soubiran, C.: 2004, PASP 116, 693

Prugniel, P., Soubiran, C.: 2001, A&A 369, 1048

Savage, B.D., Mathis, J.S. 1979, ARA&A 17, 73

Soubiran, C., Katz, D., Cayrel, R.: 1998, A&AS 133, 221

Stift, M.J., Strassmeier, K.G.: 1995, in *Stellar Surface Structure*, IAU Symp., No. 176, Poster Proc., ed. Strassmeier, K.G., 29

Strassmeier, K.G., Fekel, F.C.: 1990, A&A 230, 389

Strassmeier, K.G., Rice, J.B., Wehlau, W.H. et al.: 1993, A&A 268, 671

Strassmeier, K.G., Schordan, P.: 2000, AN 321, 277

Table 4 Coefficients of the fits $T_{\rm eff} = c_0 + c_1 r_{\rm c} + ... + c_n r_{\rm c}^n$ for the ELODIE spectra rotationally broadened to 30 km s^{-1}. The empty columns relate to the line pairs completely blended at this rotational velocity.

GIANT STARS								
LDR	1/2	3/6	5/4	7/6	9/8	11/10	12/14	13/15
c_0	5481.25	5496.39		7025.27				5695.10
c_1	−596.797	−2961.51		−5597.99				−800.163
c_2	−43.7139	4228.71		5957.99				75.3450
c_3	−48.3037	−3087.51		−2710.79				
$0.01\,\lvert\frac{\mathrm{d}T}{\mathrm{d}r_{\rm c}}\rvert_{5000\ \mathrm{K}}$	9.3	16.1		16.5				8.4
rms	0.095	0.058		0.061				0.075
LDR	13/16	17/18	21/19	21/20	23/22	24/25	26/25	
c_0	5337.08				5150.51	5190.59	5357.17	
c_1	−166.813				−825.095	−500.186	−591.566	
c_2	8.35369				70.5176	28.5439	−202.882	
c_3	−0.153085				−989.250	6.34586	92.0652	
$0.01\,\lvert\frac{\mathrm{d}T}{\mathrm{d}r_{\rm c}}\rvert_{5000\ \mathrm{K}}$	1.7				15.1	7.5	9.5	
rms	0.075				0.071	0.089	0.085	
DWARF STARS								
LDR	1/2	3/6	5/4	7/6	9/8	11/10	12/14	13/15
c_0	6432.25	5999.97		7479.52				6874.46
c_1	−3039.71	−4545.30		−3706.65				−3697.12
c_2	2161.86	6247.09		1147.46				2312.46
c_3	−692.710	−3573.28		−116.692				−595.265
$0.01\,\lvert\frac{\mathrm{d}T}{\mathrm{d}r_{\rm c}}\rvert_{5000\ \mathrm{K}}$	10.3	11.6		18.9				11.1
rms	0.066	0.046		0.051				0.079
LDR	13/16	17/18	21/19	21/20	23/22	24/25	26/25	
c_0	6082.76				5895.59	5712.75	6039.12	
c_1	−329.412				−4065.13	−1362.68	−885.351	
c_2	30.3591				5641.78	931.915	−863.622	
c_3	−0.945513				−5297.51	−312.388	527.239	
$0.01\,\lvert\frac{\mathrm{d}T}{\mathrm{d}r_{\rm c}}\rvert_{5000\ \mathrm{K}}$	1.0				20.0	5.0	10.1	
rms	0.080				0.033	0.085	0.090	

